Journal of Solid State Chemistry 181 (2008) 2306–2312

Contents lists available at ScienceDirect

Journal of Solid State Chemistry

journal homepage: www.elsevier.com/locate/jssc

Structure and phase composition of nanocrystalline $Ce_{1-x}Lu_xO_{2-y}$

Małgorzata A. Małecka, Leszek Kępiński *, Mirosław Mączka

Institute of Low Temperature and Structure Research, Polish Academy of Sciences, P.O. Box 1410, 50-950 Wrocław 2, Poland

ARTICLE INFO

Article history:
Received 6 November 2007
Received in revised form
14 March 2008
Accepted 23 May 2008
Available online 29 May 2008

Keywords:
Nanocrystals
Mixed oxides
CeO_2–Lu_2O_3
TEM
XRD
Raman
Microemulsion
Yb^{3+} emission

ABSTRACT

The microstructure and phase stability of nanocrystalline mixed oxide $Lu_xCe_{1-x}O_{2-y}$ ($x = 0$–1) are described. Nano-sized (3–4 nm) oxide particles were prepared by the reverse microemulsion method. Morphological and structural changes upon heat treatment in an oxidizing atmosphere were studied by transmission electron microscopy (TEM), X-ray diffraction (XRD), Raman and Yb^{3+} emission spectroscopy, the latter ion being present as an impurity in the Lu_2O_3 starting material. Up to 950 °C, the samples were single phase, with structure changing smoothly with Lu content from fluorite type (F) to bixbyite type (C). For the samples heated at 1100 °C phase separation into coexisting F- and C-type structures was observed for $0.35 < x < 0.7$. It was also found that addition of Lu strongly hinders the crystallite growth of ceria during heat treatment at 800 and 950 °C.

1. Introduction

Rare-earth mixed oxides find wide application as three-way catalysts [1] and in solid oxide fuel cell technology [2]. Catalytic activity of ceria-based systems is due to their ability to partially change oxidation state from 4+ to 3+ during reaction ($CeIVO_2$ to $CeIV,IIIO_{2-y}$) [3]. Structure and reduction–oxidation properties of ceria-based mixed oxides were studied by Bernal et al. [4]. Their observations indicate that Ln-doped CeO_2 nanocrystals could exhibit high activity in oxidizing reactions even at low temperatures.

The important characteristics of rare-earth mixed oxides determining their chemical properties are their crystallographic structure and stability at high temperatures. All lanthanide elements form sesquioxides (Ln_2O_3). Three crystalline types (A, B and C) have been identified for temperatures <2000 °C. The A-type oxide (La to Nd) crystallizes in the trigonal crystal system and its structure can be described in space group $P\bar{3}m1$ (164). The B-type oxide (Sm–Gd) is a monoclinic distortion of A-type and is described in $C2/m$ (12) space group. Finally, the C-type (Tb–Lu) is a cubic bixbyite ($(Fe,Mn)_2O_3$)-type structure and is described in $Ia\bar{3}$ (206) space group [5]. Ce, Pr and Tb may also form LnO_2 oxides with cubic, fluorite-type (F-type) structure and $Fm\bar{3}m$ (225) space group [5].

A number of reports have appeared on the structures of ceria-based mixed oxides ($Ce_{1-x}Ln_xO_{2-y}$, $x = Ln/(Ce+Ln)$) containing La [6,7], Nd [8,9], Sm [8,10], Eu [10], Gd [11] and Y [12,13]. In such systems, phase separation at high temperatures often limits possible applications. Existing data are however, scarce and obtained mostly for samples prepared by solid-state reaction between polycrystalline oxides at high temperature (~1400 °C). Moreover, the results are often contradictory. For Nd two phase region at $\sim 0.3 < x < \sim 0.9$ [8] was observed, but no phase separation was also reported [9]. For Sm, the phase separation occurring for $\sim 0.3 < x < \sim 0.9$ [8] as well as its lack up to $x = 0.9$ [10] was reported. In systems doped with heavy lanthanides Chavan et al. [14] reported phase separation for Er, Yb and Lu for $x = 0.5$ [14]. More complete data exists on similar CeO_2–Y_2O_3 system, where phase separation into two phases–Ce- and Y-rich oxide—over a wide composition range that was strongly dependent on heating temperature [13].

For nano-sized CeO_2-based mixed oxides one of the most important technological characteristics is texture (particle size, surface area) and structure stability at high temperatures. Additives such as La, Pr, Tb and Lu are known to hinder strongly crystallite growth during heating in oxidizing atmospheres. The inhibiting effect of Ln increases with content suggesting that additive segregation at the grain boundaries may prevent crystallite growth [15–17]. There are no however, systematic studies on the possible role of phase separation in such nano-crystalline systems.

* Corresponding author. Fax: +48 71 3441029.
E-mail address: L.Kepinski@int.pan.wroc.pl (L. Kępiński).

0022-4596/$ - see front matter © 2008 Elsevier Inc. All rights reserved.
doi:10.1016/j.jssc.2008.05.033

In this work, the structure and texture properties of nanocrystalline $Ce_{1-x}Lu_xO_{2-y}$ was studied over the whole composition range. The samples were prepared by the conventional water-in-oil microemulsion method, then heated at various temperatures (500, 800, 950 and 1100 °C) in an oxidizing atmosphere to elucidate the effect of temperature on microstructure and phase composition. Samples subjected to various treatments were thoroughly characterized by powder X-ray diffraction (XRD), transmission electron microscopy (TEM), Raman and Yb^{3+} emission spectroscopy.

2. Materials and methods

Nanoparticles of mixed $Ce_{1-x}Lu_xO_{2-y}$ oxides were prepared by precipitation using the water-in-oil (W/O) microemulsion technique described in detail in our previous paper [17]. The powder samples were dried and then preheated in oxygen flow at 500 °C for 3 h, before calcining in oxygen at 800 or 950 °C for 3 h or in static air at 1100 °C for 45 h.

True lanthanide content in $Ce_{1-x}Lu_xO_{2-y}$ samples, measured with Energy Dispersive Spectroscopy (EDAX PV 9800 spectrometer), appeared to agree within ± 0.02 with nominal content corresponding to $x = 0.10$, 0.17, 0.25, 0.30, 0.35, 0.40, 0.45, 0.50, 0.60, 0.70, 0.80 and 0.90 (Table 1).

The phase composition and lattice parameter were determined by XRD (STOE, monochromatized Cu$K\alpha_1$ radiation) with WinPLOTR program [18] used for display and analysis. Morphology and microstructure were investigated by TEM (Philips CM-20 SuperTwin operating at 200 kV and providing 0.25 nm resolution). Analysis of TEM images was made with ImageJ program [19]. Raman spectra of the samples were recorded at 2 cm^{-1} resolution using Bruker IFS-88 spectrometer. Yb^{3+} emission spectra were extracted directly from the Raman data since Yb^{3+} emission bands appear in the anti-Stokes part of the Raman spectra. Yb occurs as contamination in Lu_2O_3 used as starting material in the synthesis and according to the certificate provided by the supplier (Stanford, USA) the oxide contains less than 0.001% of Yb_2O_3. The amount of Yb^{3+} increases therefore linearly with x within of the set of $Ce_{1-x}Lu_xO_{2-y}$ samples [20,21]. The size and chemistry of Yb^{3+} ion is very similar to that of Lu^{3+} and therefore it substitutes isomorphically for Lu. Yb^{3+} may thus act as a structure probe revealing the local symmetry of Lu^{3+} ions [20,21].

3. Results and discussion

As-synthesized $Ce_{1-x}Lu_xO_{2-y}$ contains small (~4 nm) crystalline particles with narrow size distribution, similar to that observed in $Ce_{0.83}Lu_{0.17}O_{2-y}$ [17,22]. It has been previously shown that preliminary heating at 500 °C in O_2 for 3 h (standardization) removes all organics and most of nitrate groups, while treatment in O_2 at above 800 °C is necessary to get rid of carbonate groups [17]. Chemical formula with undetermined "y" factor was used, instead of stoichiometric $Ce_{1-x}Lu_xO_{2-x/2}$, because a fraction of Ce ions at the surface of particles may exist as Ce^{+3} even in nonreduced ceria [23]. The Ce^{3+}/Ce^{4+} ratio may be close to 1 for very small particles (<2 nm) but decreases to ~0.01 for larger ones (>15 nm) [24]. We assume therefore that the presence of very small fraction of Ce^{3+} in the samples heated in oxidizing atmosphere at temperatures ⩾800 °C can be ignored.

3.1. XRD analysis

XRD patterns of the samples heated at 800 °C (not shown) and 950 °C in O_2 for 3 h (Fig. 1A) were similar and revealed a continuous transformation of the structure from fluorite ($Fm\bar{3}m$) in the range $0<x<0.5$ to bixbyite ($Ia\bar{3}$) in range $0.6<x<1$. Prolonged heating of $Ce_{0.55}Lu_{0.45}O_{2-y}$ and $Ce_{0.5}Lu_{0.5}O_{2-y}$ at 950 °C in O_2 for 15 h did not cause any shift or splitting of XRD reflections indicating phase stability at this temperature. The patterns of pure CeO_2 ($x = 0$) and Lu_2O_3 ($x = 1$) fitted well the reference data: ICDD PDF No. 00-034-0394 and 00-012-0728, respectively. Addition of Lu decreased the cell parameter of parent cubic CeO_2 over the whole x range (for bixbyite-type structure half of the cell parameter was taken) (Fig. 1B), as expected from the effective ionic radii ($Ce^{4+} = 0.092$ nm, $Lu^{3+} = 0.085$ nm [25]). Closer look at Fig. 1B reveals, however clear deviations from Vegard's rule and three regions can be distinguished, which also correlates with systematic changes in relative intensities of the $(311)_F/(111)_F$, or $(622)_C/(222)_C$ reflections (Fig. 1C). In the first region, $x<0.25$, the change of cell parameter is the slowest and $(311)_F/(111)_F$ ratio is close to that in CeO_2. In the second region, $0.25<x<0.5$, together with faster decrease in cell parameter there is a continuous change in relative intensities of reflections. Finally in third region, $x>0.5$ the change of the cell parameter is the fastest and intensity ratios $(311)_F/(111)_F$, or $(622)_C/(222)_C$, are close to those observed for Lu_2O_3.

Deviations from Vegard's rule have been reported in other $Ce_{1-x}Ln_xO_{2-y}$ systems, where Ln = La [26], Y [12], Gd [27]. As possible explanation of this deviation contraction of the unit cell volume of the fluorite structure by coalescence of vacancies was proposed [7]. In the intermediate x region, this deviation gets even larger since there is transformation from fluorite to bixbyite, as indicated by the change in relative intensities of reflections (Fig. 1C). The F–C structure change with x, occurring without phase separation for the $Ce_{1-x}Lu_xO_{2-y}$ heated at 800 and 950 °C, proceeded through an intermediate defect cubic (F-type) structure existing for $0.25<x<0.5$. In the intermediate F-type phase, oxygen vacancies can be ordered to form superstructure with decreasing oxygen concentration in the oxide [28]. The deviations

Table 1
Composition and mean crystallite sizes of $Ce_{1-x}Lu_xO_{2-y}$ samples subjected to various treatments

Thermal treatment	$Ce_{1-x}Lu_xO_{2-y}$ [x]													
Nominal composition	0	0.10	0.17	0.25	0.30	0.35	0.40	0.45	0.50	0.60	0.70	0.80	0.90	1
Measured composition[a]	–	0.08	0.15	0.26	0.28	0.36	0.38	0.45	0.50	0.62	0.71	0.80	0.90	–
	TEM mean size (volume weighted) d (nm)													
800 °C/3 h O_2	25	25	16	–	16	–	–	9	8	12	13	11	14	21
950 °C/3 h O_2	81	44	23	–	30	–	–	20	26	33	25	22	24	19
	XRD mean size (Scherrer formula) d (nm)													
800 °C/3 h O_2	28	21	14	15	16	12	10	9	8	11	10	8	9	10
950 °C/3 h O_2	64	32	22	21	22	20	18	18	19	17	17	13	14	14

[a] Measured with EDS; x = at% Lu/(at% Lu+at% Ce), accuracy ± 0.01.

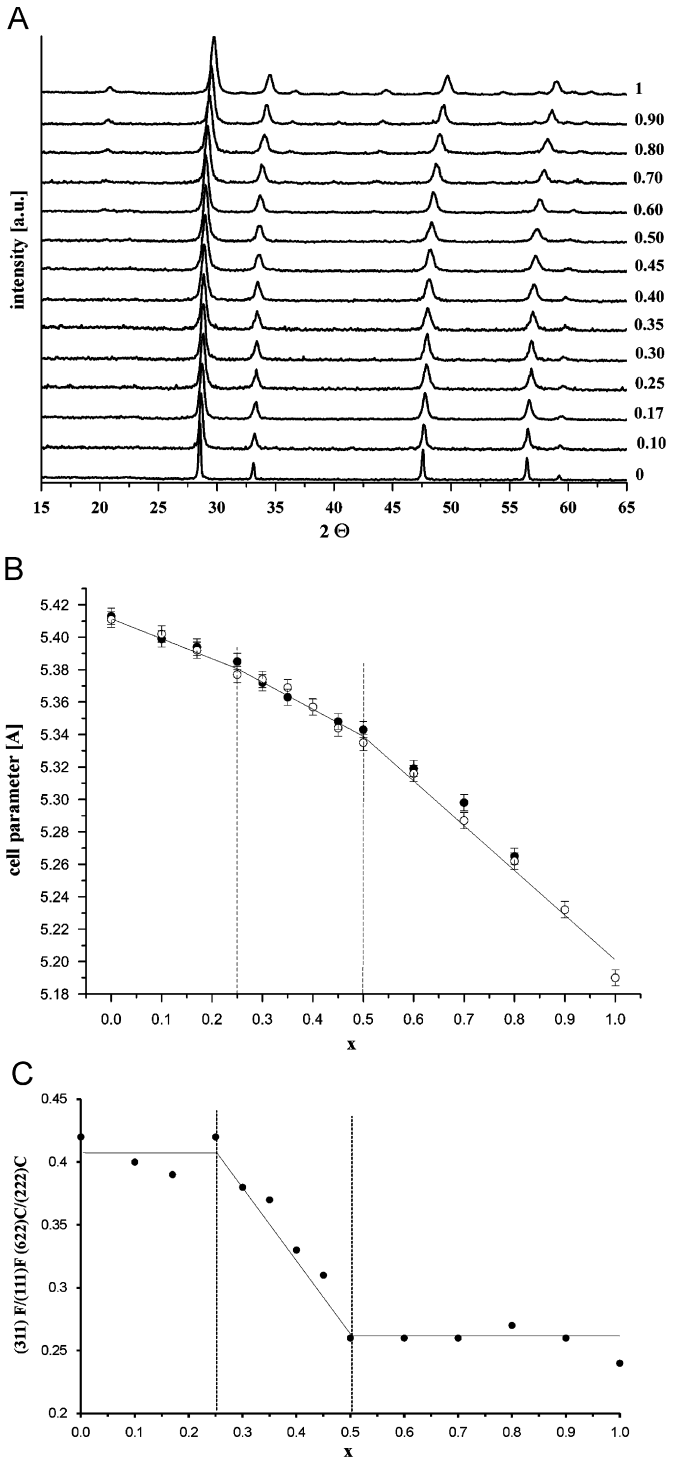

Fig. 1. XRD patterns of $Ce_{1-x}Lu_xO_{2-y}$ heated at 950 °C for 3 h in O_2 (A), cell parameter for samples heated at (●) 800 °C and (○) 950 °C for 3 h in O_2 (B) and dependence of the intensity ratio of XRD reflections, $(311)_F/(111)_F$ or $(622)_C/(222)_C$, on x for $Ce_{1-x}Lu_xO_{2-y}$ heated at 950 °C for 3 h in O_2 (C).

from linearity for $x>0.5$ may be ascribed to different partitioning of Ce and Lu over 8*d* and 24*b* sites in bixbyite [29,30].

Mean crystallite sizes calculated from XRD line broadening (Scherrer formula) and measured from TEM are given in Table 1. It appears that for the samples heated at 800 and 950 °C there is a correlation between crystallite size and Lu content (x). Heating at 800 °C caused 5-fold increase of the mean crystallite size of CeO_2 while a 1.5–4-fold increase was observed for the doped samples. At 950 °C, the growth is more than 10 fold for CeO_2 and 3–5-fold for $Ce_{1-x}Lu_xO_{2-y}$. The inhibiting effect of Lu dopant on crystallite growth of CeO_2 is the highest in the $0<x<0.25$ range and then saturates.

Phase separation was observed as a function of Lu content in $Ce_{1-x}Lu_xO_{2-y}$ heated at 1100 °C for 45 h in air (Fig. 2A). The left hand panel shows a region of XRD patterns where the (431) reflection characteristic for C-type oxide is expected. It is seen that for $x\geqslant 0.5$, the reflection becomes visible and then grows and shifts towards higher angles. In the central panel, another region of the patterns is shown where $(022)_F$ and $(044)_C$ reflections occur, while the multiphase nature of certain samples summarized in right-hand panel. Two main phases F-type and C-type were observed for $0.35<x<0.7$ and additionally a third $C^{\#}$-type phase occurred for $0.5<x<0.7$. The intensity of the XRD reflections of the $C^{\#}$ phase decreased with increasing heat treatment time to 75 h indicating that the phase is probably metastable. The existence of $C^{\#}$ phase may be due to different partitioning of Ce and Lu over 8*d* and 24*b* sites in bixbyite [29,30]. Analysis of the variation of the lattice parameter with Lu content (Fig. 2B) indicates that up to 35 mol% Lu dissolves in CeO_2 and the solubility of Ce in $LuO_{1.5}$ is 20 mol%. These solubility limits are bigger than those observed for $Ce_{1-x}Y_xO_{2-y}$ [13,31,32].

The only information on phase composition of Lu_2O_3–CeO_2 system by Chavan et al. [14], reported phase separation for the oxide with the initial composition $Ce_{0.5}Lu_{0.5}O_{1.75}$ heated at 1400 °C for 48 h into fluorite and bixbyite. Many papers reported phase relations for CeO_2–Y_2O_3 system, which have the same structure of single oxides and bears a resemblance to CeO_2–Lu_2O_3 [12,13,33,34]. The phase diagram of $Ce_{1-x}Y_xO_{2-y}$ shows phase separation into solid solutions of Y_2O_3 in CeO_2 (F-type) and CeO_2 in Y_2O_3 (C-type), over a wide x-range. However, the two-phase area depends upon heating temperature from $0.1<x<0.8$ for 900 °C to $0.25<x<0.7$ for 1700 °C [13]. Within the range of existence of the solid solution the lattice parameter changes in accord with Vegard's rule [13,31,32].

3.2. Raman analysis

Fig. 3 shows the Raman spectra of $Ce_{1-x}Lu_xO_{2-y}$ mixed oxides ($0<x<1$) heated in oxygen at 950 °C for 3 h. Spectra of the samples treated at 800 and at 1100 °C were similar and are not shown. The spectra have been processed (background subtraction) and normalized to the strongest band. An effect of increasing heat treatment temperature on the Raman spectra (Fig. S1 in the supplementary materials) was some sharpening of the bands, especially for the samples with $x\cong 0.5$, and the development of bands characteristic of bixbyite phase. This observation correlates with phase separation at high temperature revealed by XRD.

The spectrum of pure CeO_2 contains a strong, single band at 465 cm^{-1} assigned to F_{2g} mode in fluorite structure [35]. With the addition of Lu important changes in the spectra occurred. Already for $x=0.1$ strong attenuation of the F_{2g} band was observed with its simultaneous shift to 467 cm^{-1} and broadening on the high wavenumber side. Moreover, weak new bands appeared at 251, 492 (*sh*), 560 and 603 cm^{-1}. For $x=0.25$ and 0.30, intensity of the F_{2g} band again decreased but its width increased strongly. The main band shifted to 473 cm^{-1} and the shoulder at 492 cm^{-1} gained some intensity. The position of the weak bands changed also to 255, 561 and 609 cm^{-1}. For $x=0.35$, a new weak band occurred at 389 cm^{-1} and its relative intensity increased with x up to 1. At the same time, the intensity of the main F_{2g} band at 473 cm^{-1} decreased in relation to and that of 492 cm^{-1} band. There is also an increase in intensity of the broad band at 611 cm^{-1}. For $x=0.8$, intensity of the whole Raman spectrum was

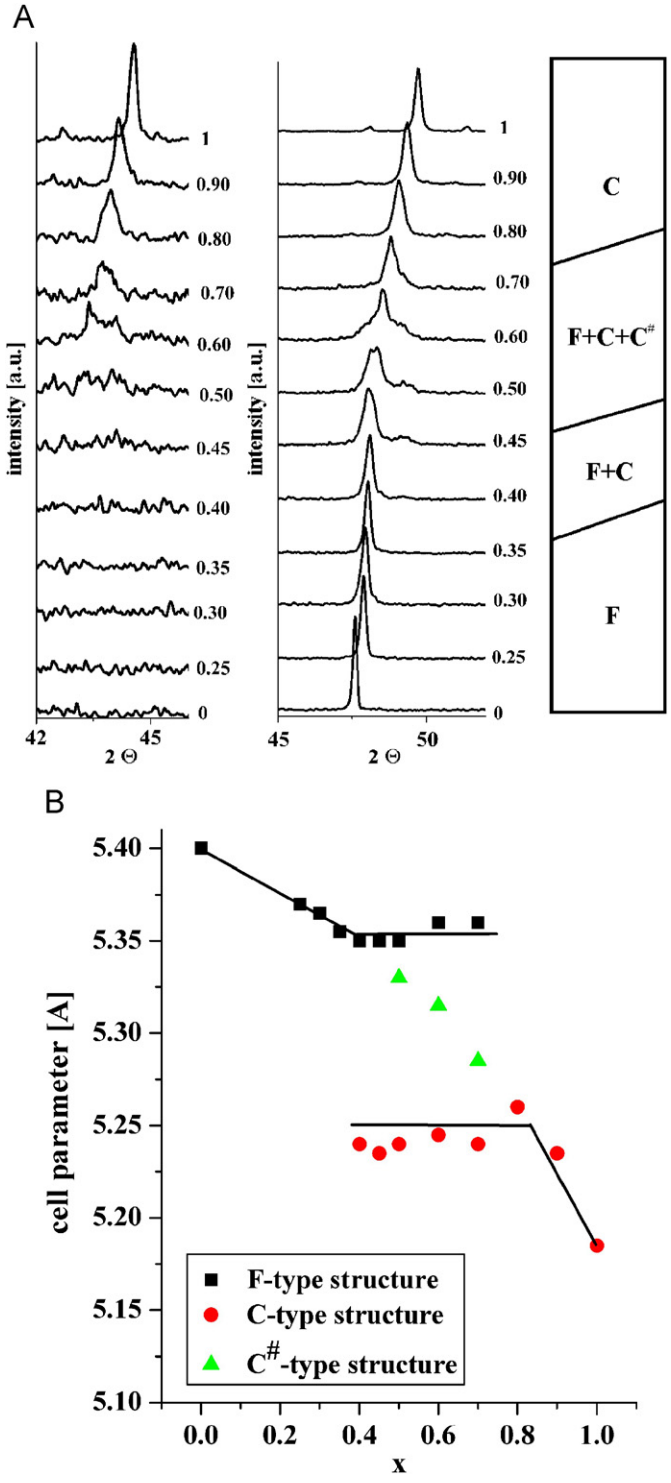

Fig. 2. Characteristic regions of XRD patterns of $Ce_{1-x}Lu_xO_{2-y}$ heated at 1100 °C for 45 h in air and proposed phase composition (see text for explanation) (A), cell parameter of $Ce_{1-x}Lu_xO_{2-y}$ heated at 1100 °C for 45 h in air (B).

very weak and there was no evidence for the band corresponding to fluorite structure. For $x = 0.9$ and 1, there was significant growth in intensity of the band at 382 (392) cm^{-1} characteristic for C-Lu_2O_3 [36]. An interesting feature of the spectra of the samples with high Lu content ($0.5 < x < 0.9$) is the strong, broad band at approximately 620 cm^{-1}. This band occurs also as a weak feature in Raman spectra of bulk Lu_2O_3 [36].

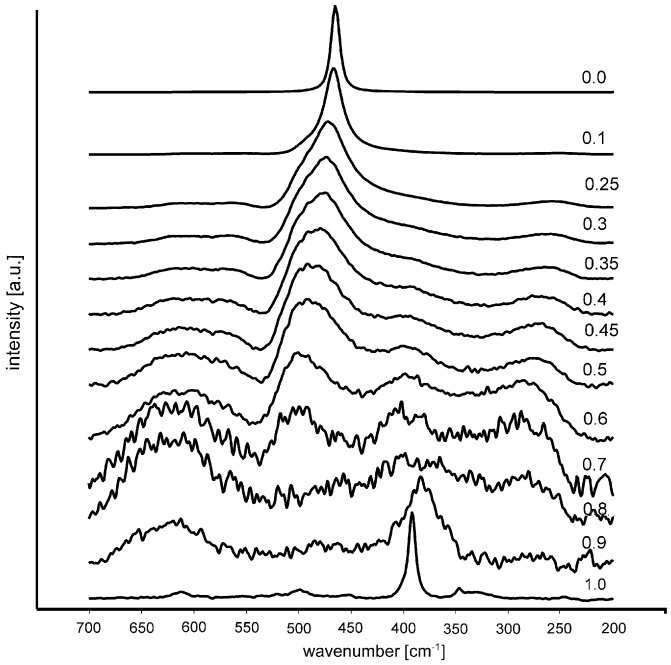

Fig. 3. Raman spectra of $Ce_{1-x}Lu_xO_{2-y}$ mixed oxides ($0 < x < 1$) heated in oxygen at 950 °C for 3 h.

Strong weakening and broadening of the main Raman bands of CeO_2 upon addition of guest lanthanide ions arises from structure disorder and changes of symmetry [37]. On the other hand, the appearance of additional weak bands at ~250 and 560 cm^{-1} is explained as the effect of tetragonal distortion of the cubic fluorite sub-lattice [38]. An alternative explanation for the band at 560 cm^{-1} could be the presence of oxygen vacancies generated upon substitution of Ce^{4+} with Lu^{3+}. Occurrence of such band upon doping CeO_2 with trivalent ions is well known [37,39,40]. Finally, the origin of a weak band at ~600–630 cm^{-1} is unclear. A weak band at ~600 cm^{-1} is known to occur in undoped nanocrystalline CeO_2 [40,41] and could be assigned to intrinsic O^{2-} vacancies originating from increased oxygen nonstoichiometry of nanocrystalline ceria powders. The extension of the band towards higher wavenumbers (610–630 cm^{-1}) in samples strongly doped with Lu may suggest its connections also with special defect modes present in bixbyite. The shift of the main fluorite F_{2g} band towards higher wavenumbers with x is the consequence of the lattice shrinkage (Gruneisen shift) [37], and correlates with the shift of the weak band at ~250 cm^{-1} assigned to a second-order 2TA mode [42]. The same effect explains also shift of the main band of Lu_2O_3 with addition of Ce, although the direction of the shift is now opposite as the lattice expands.

Careful analysis of the spectra revealed that apart from broadening and shift, the main fluorite F_{2g} band contains a shoulder at ~490 cm^{-1} that is clearly visible for $x \geqslant 0.25$. With increasing x the band dominates the spectra because of weakening of the main 465 cm^{-1} band, but its position does not change. The origin of this band is unclear and will be discussed further in the paper.

For very high Lu contents, rapid decline of the main Lu_2O_3 band at 392 cm^{-1} together with its broadening and shift were noticed with increasing Ce content, much more pronounced that for Lu doping into CeO_2. The reason must be very strong distortion of Lu_2O_3 lattice upon Ce substitution. There are two possibilities of such substitution: either with Ce^{3+} or with Ce^{4+}. In the first case, there is large misfit in ionic radii (0.086 nm Lu^{3+} vs. 0.101 nm Ce^{3+}) but there is no need for charge compensation. In the second case,

ionic radii are very similar (0.086 nm vs. 0.087 nm) but additional O^{2-} ions must be added to provide charge neutrality. In both cases, severe lattice deformation occurs. UV/vis spectroscopy data for Lu_2O_3 single crystals doped with 0.26 mol% Ce and heated in oxidizing atmosphere excluded, however the presence of significant amount of Ce^{3+} [43].

3.3. Yb^{3+} emission spectroscopy

Fig. 4 shows emission spectra of Yb^{3+} ions present as impurity in $Ce_{1-x}Lu_xO_{2-y}$ heated in oxygen at 950 °C for 3 h. Spectra of the samples treated at 800 and at 1100 °C (not shown) were similar what is in apparent contradiction with XRD data where clear differences due to phase separation were observed. The abscissa axes in Fig. 4 have been transformed to show directly wavenumbers of the emitted radiation. The transformation was as follows: wavenumber (cm^{-1}) = 9398 (cm^{-1})—Raman shift (cm^{-1}), where 9398 cm^{-1} is the wavenumber of excitation radiation (1064 nm). The spectra have been normalized to maximum intensity in order to better visualize observed changes. It appears that the shape of the emission spectra of Yb^{3+} depends strongly on composition (Lu content) and to some extent also on the temperature of heat treatment (Fig. S2); the samples heated at 950 °C will be described in detail. For $x = 0.1$, the spectrum contains strong band at 10285 cm^{-1} and three weak bands at 10242, 10175 and 10348 cm^{-1} and is similar to that of CeO_2 doped with 1% Yb, though the main band is slightly shifted by 4 cm^{-1}. For $x > 0.3$, the intensity of the band at 10242 cm^{-1} increases at the expense of the main band at 10285 cm^{-1} so, that at $x = 0.7$ the bands are roughly the same. At even higher x, the spectra resemble those of Yb^{3+} in Lu_2O_3 or in Yb_2O_3 (cf. Fig. 4) [21,44]. It appears therefore, that Lu ions in CeO_2 must be in local environment resembling that in Lu_2O_3. XRD and TEM did not provide any evidence for the existence of crystalline microdomains with C-type structure for $x \leqslant 0.4$ so that it must be assumed that there are unordered regions enriched in Lu^{3+} ions, e.g. at the surface of ceria crystallites.

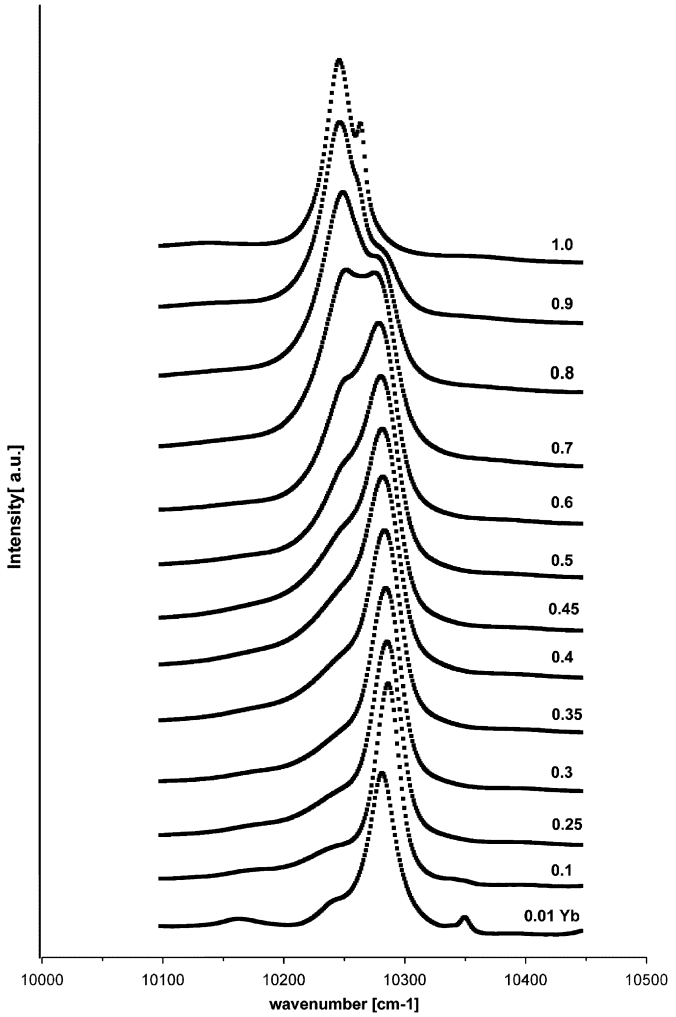

Fig. 4. Yb^{3+} emission bands of $Ce_{1-x}Lu_xO_{2-y}$ mixed oxides ($0 < x < 1$) heated in oxygen at 950 °C for 3 h. For comparison, the spectrum of Yb^{3+} ions in $Ce_{0.99}Yb_{0.01}O_{2-y}$ is shown.

The dependence of the emission spectra on the temperature of heat treatment is less pronounced (Fig. S2). For high Lu content ($x \geqslant 0.6$) only some sharpening of the bands is observed that may be explained by enhanced ordering of the samples (growth of crystallite size). However, for low and medium Lu content ($x \leqslant 0.5$), a significant decline in intensity of the low wavenumber band at 10242 cm^{-1} with temperature was noticed, especially above 950 °C. This band is characteristic for Yb^{3+} emission in bixbyite-type oxides (Lu_2O_3 and Yb_2O_3). A possible interpretation of this observation could be effect of surface segregation reported in $Ce_{1-x}Ln_xO_{2-y}$ (Ln = La [6,26], Pr [15]). For low and medium Lu content, the surface region $Ce_{1-x}Lu_xO_{2-y}$ crystallites is enriched in Lu (and thus also Yb) so that local environment of emitting Yb^{+3} ions resemblances that in C-type oxide. Prolonged heating at 1100 °C causes "homogenization" of the samples i.e. diffusion of Yb^{3+} ions into CeO_2 matrix. This could be responsible also for disappearance of the inhibiting action of Lu on the crystallite growth.

3.4. TEM analysis

Results of measurements of crystallite sizes from HRTEM images are summarized in Fig. S3 and in Table 1. Volume weighted mean crystallite sizes ($\Sigma n_i d_i^4 / \Sigma n_i d_i^3$) were calculated instead of simple arithmetic mean to enable comparison with the mean crystallite sizes calculated from XRD data with the Scherrer formula [45]. In accordance with XRD data, it appears that for the samples heated at 800 and 950 °C addition of Lu hindered the crystallite growth. As an example, Fig. 5 compares images of the samples with $x = 0.1$ and 0.5 heated at 800 °C. The effect is strong for Lu content up to $x = 0.3$ and than saturates. This observation agrees with literature data [15–17] and according to Borchert et al. [16] it may be explained by segregation of the dopant ions at the surface of ceria crystallites. Recently, the surface enrichment in trivalent Ln component was reported for $Ce_{1-x}Ln_xO_{2-y}$ where Ln = La [6], Pr [15]. Extensive crystal growth up to 100 nm was observed for all samples heated at 1100 °C in air for 45 h, irrespective of composition. It means that an inhibiting effect of Lu-ions addition on ceria crystal growth vanishes at high temperatures, due to "homogenization" of the samples mentioned above.

Very weak ~0.76 nm fringes were observed in HRTEM images (or more clearly in corresponding FFT patterns) for $Ce_{1-x}Lu_xO_{2-y}$ with $x = 0.45$ and 0.5 heated at 950 °C for 3 h (Fig. 6A). The fringes could be assigned to superstructure 1/4{220} reflections occurring due to doubling of the fluorite cell as a result of oxygen vacancy ordering. This observation correlates with unusual ratios of intensities of XRD reflections for samples in the range $0.3 < x < 0.5$. The existence of such phase may be also inferred from the Raman spectra, where splitting of the main F_{2g} band at ~460 cm^{-1} occurred for $x \geqslant 0.25$. The high lying component

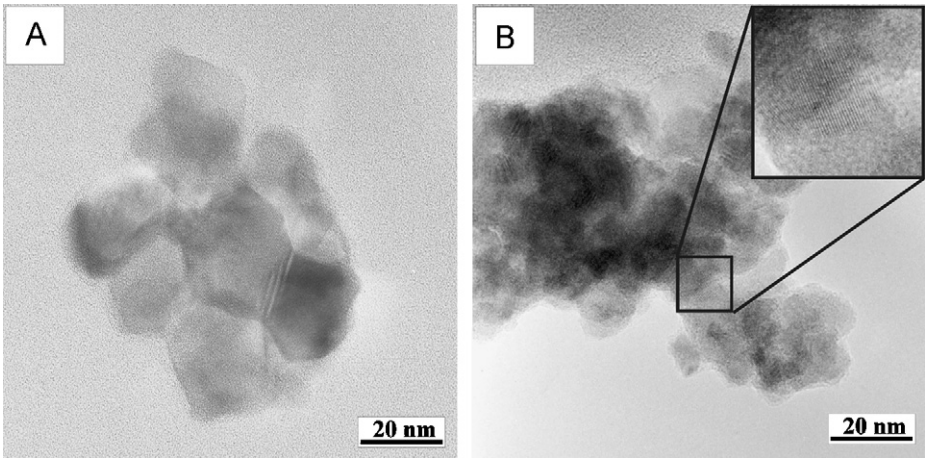

Fig. 5. HRTEM images of $Ce_{1-x}Lu_xO_{2-y}$ with (A) $x = 0.1$ and (B) $x = 0.5$ heated at 800 °C for 3 h in O_2.

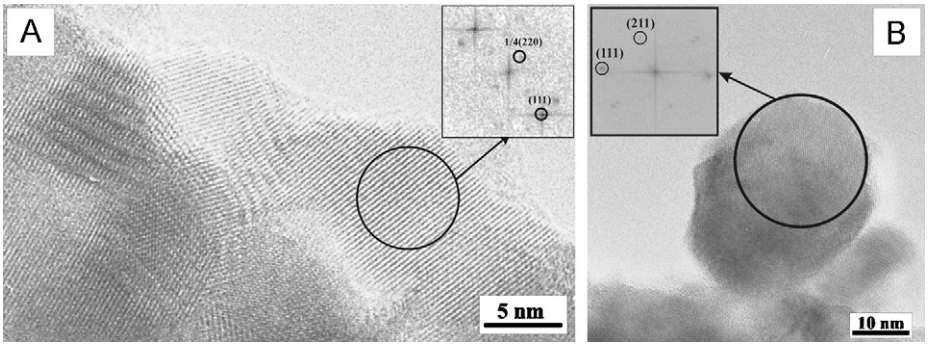

Fig. 6. HRTEM images and FFT patterns of $Ce_{0.55}Lu_{0.45}O_{2-y}$ heated at 950 °C for 3 h in O_2. Crystallites with fluorite superstructure (A) and bixbyite structure (B) are shown.

($\sim$490 cm^{-1}) of F_{2g} band could be observed up to $x = 0.7$, whereas the low laying one faded completely at $x \geqslant 0.5$. In an earlier study, of the CeO_2–Y_2O_3 system [12,34,46], observation of 1/4{220} satellites for intermediate concentrations of dopant ions ($x \cong 0.5$) led the authors to propose the fluorite-type superstructure with a periodicity of double F-unit cell. The superstructure was interpreted as a result of oxygen vacancy ordering (with "C-type domains dispersed in a fluorite-type matrix").

Recently, it has been reported that prolonged exposure (several minutes) to electron beam in TEM may cause partial reduction of ceria nanocrystals with formation of superstructure, similar to this reported in this work [47]. We agree that partial reduction of multivalent oxides is possible in TEM due to high vacuum and impact of high-energy electrons [48]. However, we reject the possibility that superstructure fringes observed for $Ce_{1-x}Lu_xO_{2-y}$ with $x = 0.45$ and 0.5 heated at 950 °C for 3 h (Fig. 6) could be artifacts due to electron beam interaction. The reason is that under normal working conditions we never observed such superstructure fringes for samples with low Lu content and moreover our TEM results correlates with XRD and Raman data.

In accordance with Raman data, FFT analysis of HRTEM images revealed the occurrence of 0.42 nm fringes (corresponding to {211} lattice planes of C-type structure) in some crystallites in the $Ce_{0.55}Lu_{0.45}O_{2-y}$ and $Ce_{0.5}Lu_{0.5}O_{2-y}$ samples after heating at 950 °C for 3 h in O_2 (Fig. 6B). It may indicate that locally, crystallites with C-type structure may occur before they manifest in XRD patterns. For samples with higher Lu content $0.6 < x < 0.9$ heated at 800 and 950 °C crystallites with 0.42 nm lattice fringes were frequently observed, in accordance with XRD and Raman data. The same conclusion can be drawn from SAED patterns showing increasing number of 0.42 nm reflections with x increasing from 0.6 to 1.

4. Conclusions

Nano-sized (4–5 nm) particles of $Ce_{1-x}Lu_xO_{2-y}$ in range $0 < x < 1$, were synthesized for the first time using a W/O microemulsion method. All mixed oxides were single phase materials up to temperature of 950 °C having the fluorite structure (F-type) in range $0 < x < 0.5$ and bixbyite structure (C-type) in range $0.6 < x < 1$. Phase separation was observed at 1100 °C within composition range $0.35 < x < 0.7$. Two main (F- and C-type) phases were present over this range with additional metastable of $C^{\#}$-type phase existing for $0.5 < x < 0.7$.

XRD and TEM data showed that Lu additive hindered strongly the crystallite growth of ceria during heating in oxidizing atmosphere up to 950 °C. Emission spectra of Yb^{3+} ions present as impurity indicate that the segregation of the dopant to the crystallite surface may be responsible for this effect.

Acknowledgments

This work was financially supported by the Polish Ministry of Science and Higher Education (Grant no. N205 0326 33). The authors thank Mrs. Z. Mazurkiewicz for valuable help with preparation of the samples and Mrs. E. Bukowska for XRD work.

Appendix A. Supplementary materials

The online version of this article contains additional supplementary data. Please visit doi:10.1016/j.jssc.2008.05.033.

References

[1] S. Bernal, G. Blanco, M. Cauqui, P. Corchado, J. Pintado, J. Rodriguez-Izquierdo, Chem. Commun. (1997) 1545–1546.
[2] N. Laosiripojana, S. Assabumrungrat, Appl. Catal. B 66 (2006) 29–39.
[3] E. Aneggi, C. de Leitenburg, G. Dolcetti, A. Trovarelli, Catal. Today 114 (2006) 40–47.
[4] S. Bernal, G. Blanco, F. Botana, J. Gatica, J. Perez-Omil, J. Pintado, J. Rodriguez-Izquierdo, J. Alloys Compds. 207/208 (1994) 196–200.
[5] G. Adachi, N. Imanaka, Chem. Rev. 98 (1998) 1479–1514.
[6] V. Belliere, G. Joorst, O. Stephan, F. de Groot, B. Weckhuysen, J. Phys. Chem. B 110 (2006) 9984–9990.
[7] J. Bae, W. Choo, C. Lee, J. Eur. Ceram. Soc. 24 (2004) 1291–1294.
[8] H. Nitani, T. Nakagawa, M. Yamanouchi, T. Osuki, M. Yuya, T. Yamamoto, Mater. Lett. 58 (2004) 2076–2081.
[9] Y. Ikuma, E. Shimada, N. Okamura, J. Am. Ceram. Soc. 88 (2005) 419–423.
[10] B. Mandal, V. Grover, A. Tyagi, Mater. Sci. Eng. A 430 (2006) 120–124.
[11] V. Grover, A. Tyagi, Mater. Res. Bull. 39 (2004) 859–866.
[12] R. Wallenberg, R. Withers, D. Bevan, J. Thompson, P. Barlow, B. Hyde, J. Less-Common Met. 156 (1989) 1–16.
[13] V. Longo, L. Podda, J. Mater. Sci. 16 (1981) 839–841.
[14] S. Chavan, A. Tyagi, Mater. Sci. Eng. A 404 (2005) 57–63.
[15] M. Luo, Z. Yan, L. Jin, M. He, J. Phys. Chem. B 110 (2006) 13068–13071.
[16] H. Borchert, Y. Frolova, V. Kaichev, I. Prosvirin, G. Alikina, A. Lukashevich, V. Zaikovskii, E. Moroz, S. Trukhan, V. Ivanov, E. Paukshtis, V. Bukhtiyarov, V. Sadykov, J. Phys. Chem. B 109 (2005) 5728–5738.
[17] M. Małecka, L. Kępiński, W. Mišta, Appl. Catal. B 74 (2007) 290–298.
[18] T. Roisnel, J. Rodríguez-Carvajal, WinPLOTR: a Windows tool for powder diffraction patterns analysis, Materials Science Forum, in: R. Delhez, E.J. Mittenmeijer (Eds.), Proceedings of the Seventh European Powder Diffraction Conference (EPDIC 7), 2000, pp. 118–123.
[19] W. Rasband, ImageJ, US National Institutes of Health, Bethesda, MD, USA 〈http://rsb.info.nih.gov/ij/〉, 1997–2005.
[20] T. Biljan, S. Roncevic, Z. Meic, K. Jurcic, E. Mestrovic, Spectrochim. Acta Part A 63 (2006) 501–505.
[21] L. Kępiński, M. Maczka, J. Hanuza, Spectrochim. Acta Part A 65 (2006) 1025–1029.
[22] M. Małecka, L. Kępiński, W. Mišta, J. Alloys Compds. 451 (2008) 567–570.
[23] S.R. Gilliss, J. Bentley, C.R. Carter, Appl. Surf. Sci. 241 (2005) 61–67.
[24] F. Zhang, P. Wang, J. Koberstein, S. Khalid, S. Chan, Surf. Sci. 563 (2004) 74–82.
[25] R. Shannon, Acta Crystallogr. A 32 (1976) 751–767.
[26] K. Ryan, J. McGrath, R. Farrell, W. O'Neill, C. Barnes, M. Morris, J. Phys.: Condens. Matter 15 (2003) L49–L58.
[27] Z. Tianshu, P. Hing, H. Huang, J. Kilner, Solid State Ionics 148 (2002) 567–573.
[28] D. Ou, T. Mori, F. Ye, T. Kobayashi, J. Zou, G. Auchterlonie, J. Drennan, Appl. Phys. Lett. 89 (2006) 171911_1–171911_3.
[29] Z.K. Heiba, Y. Akin, W. Sigmund, Y.S. Hascicek, J. Appl. Crystallogr. 36 (2003) 1411–1416.
[30] M.R. Levy, C.R. Stanek, A. Chroneos, R.W. Grimes, Solid State Sci. 9 (2007) 588–593.
[31] L. Li, O. Van Der Biest, P. Wang, J. Vleugels, W. Chen, S. Huang, J. Eur. Ceram. Soc. 21 (2001) 2903–2910.
[32] E. Andrievskaya, A. Samelyuk, L. Lopato, Powder Metall. Metal Ceram. 41 (2002) 63–71.
[33] N. Gabbitans, J. Thompson, R. Withers, A. Rae, J. Solid State Chem. 115 (1995) 23–36.
[34] R. Withers, J. Thompson, N. Gabbitans, L. Wallenberg, T. Welberry, J. Solid State Chem. 120 (1995) 290–298.
[35] W. Weber, K. Hass, J. McBride, Phys. Rev. B 48 (1993) 178–185.
[36] L. Laversenne, Y. Guyot, C. Goutaudier, M. Cohen-Adad, G. Boulon, Opt. Mater. 16 (2001) 475–483.
[37] J. McBride, K. Hass, B. Poindexter, J. Appl. Phys. 76 (1994) 2435–2441.
[38] X. Wang, J. Hanson, J. Rodriguez, C. Belver, M. Fernández-García, J. Chem. Phys. 122 (2005) 154711.
[39] A. Nakajima, A. Yoshihara, M. Ishigame, Phys. Rev. B 50 (1994) 13297–13307.
[40] Z. Dohcevic-Mitrovic, M. Grujic-Brojcin, M. Scepanovic, Z. Popovic, S. Boskovi, B. Matovic, M. Zinkevich, F. Aldinger, J. Phys.: Condens. Matter 18 (2006) S2061–S2068.
[41] M. Hernandez-Alonso, A. Hungría, A. Martínez-Arias, J. Coronado, J. Conesa, J. Soria, M. Fernández-García, Phys. Chem. Chem. Phys. 6 (2004) 3524–3529.
[42] J. Spanier, R. Robinson, F. Zhang, S. Chan, I. Herman, Phys. Rev. B 64 (2001) 245407.
[43] U. Happek, S.A. Basun, J. Choi, J.K. Krebs, M. Raukas, J. Alloys Compds. 303–304 (2000) 198–206.
[44] K. Petermann, G. Huber, L. Fornasiero, S. Kuch, E. Mix, V. Peters, S. Basun, J. Lumin. 87–89 (2000) 973–975.
[45] R. Matyi, L. Schwartz, J. Butt, Catal. Rev.-Sci. Eng. 29 (1) (1987) 41–99.
[46] R. Withers, R. Wallenberg, D. Bevan, J. Thompson, B. Hyde, J. Less-Common Met. 156 (1989) 17–27.
[47] T. Akita, M. Okumura, K. Tanaka, M. Kohyama, M. Haruta, Catal. Today 117 (2006) 62–68.
[48] D.S. Su, Anal. Bioanal. Chem. 374 (2002) 732–735.